

Baroj Abdulkarim,<sup>1</sup> Marc Nicolino,<sup>2,3,4</sup> Mariana Igoillo-Esteve,<sup>1</sup> Mathilde Daures,<sup>5,6</sup> Sophie Romero,<sup>5,6</sup> Anne Philippi,<sup>5,6</sup> Valérie Senée,<sup>5,6</sup> Miguel Lopes,<sup>1</sup> Daniel A. Cunha,<sup>1</sup> Heather P. Harding,<sup>7</sup> Céline Derbois,<sup>8</sup> Nathalie Bendelac,<sup>2</sup> Andrew T. Hattersley,<sup>9</sup> Décio L. Eizirik,<sup>1</sup> David Ron,<sup>7</sup> Miriam Cnop,<sup>1,10</sup> and Cécile Julier<sup>5,6</sup>



## A Missense Mutation in *PPP1R15B* Causes a Syndrome Including Diabetes, Short Stature, and Microcephaly

*Diabetes* 2015;64:3951–3962 | DOI: 10.2337/db15-0477

**Dysregulated endoplasmic reticulum stress and phosphorylation of eukaryotic translation initiation factor 2 $\alpha$  (eIF2 $\alpha$ ) are associated with pancreatic  $\beta$ -cell failure and diabetes. Here, we report the first homozygous mutation in the *PPP1R15B* gene (also known as constitutive repressor of eIF2 $\alpha$  phosphorylation [CReP]) encoding the regulatory subunit of an eIF2 $\alpha$ -specific phosphatase in two siblings affected by a novel syndrome of diabetes of youth with short stature, intellectual disability, and microcephaly. The R658C mutation in *PPP1R15B* affects a conserved amino acid within the domain important for protein phosphatase 1 (PP1) binding. The R658C mutation decreases PP1 binding and eIF2 $\alpha$  dephosphorylation and results in  $\beta$ -cell apoptosis. Our findings support the concept that dysregulated eIF2 $\alpha$  phosphorylation, whether decreased by mutation of the kinase (*EIF2AK3*) in Wolcott-Rallison syndrome or increased by mutation of the phosphatase (*PPP1R15B*), is deleterious to  $\beta$ -cells and other secretory tissues, resulting in diabetes associated with multisystem abnormalities.**

The molecular mechanisms contributing to pancreatic  $\beta$ -cell dysfunction and apoptosis in diabetes remain poorly understood. Accumulating evidence suggests that

endoplasmic reticulum (ER) stress and aspects of the response to it contribute to  $\beta$ -cell failure both in type 1 and type 2 diabetes (1–6). ER stress is defined as an imbalance between unfolded protein load in the ER and the organelle's functional capacity. This activates an ER stress response, also known as the unfolded protein response (UPR), which reduces protein load and increases ER folding capacity. The UPR is an adaptive response, particularly important for the survival of cells with a high secretory capacity such as pancreatic  $\beta$ -cells. The UPR is triggered by the activation of ER transmembrane proteins that sense the misfolded protein accumulation in the ER lumen and transduce the signal to the cytoplasm. One of the canonical ER stress transducers is protein kinase R-like endoplasmic reticulum kinase (PERK, encoded by *EIF2AK3*). PERK phosphorylates the eukaryotic translation initiation factor 2 $\alpha$  (eIF2 $\alpha$ ) and attenuates protein translation to lessen the burden of the stressed ER (1,7). The effector pathway downstream of PERK is tightly regulated by eIF2 $\alpha$  dephosphorylation carried out by a holo-phosphatase complex consisting of a common catalytic subunit, protein phosphatase 1 (PP1), and a substrate-specific regulatory subunit, PPP1R15. Two such regulatory subunits are known: the constitutive repressor of eIF2 $\alpha$  phosphorylation (CReP), encoded by *PPP1R15B*,

<sup>1</sup>ULB Center for Diabetes Research, Université Libre de Bruxelles, Brussels, Belgium

<sup>2</sup>Hôpital Femme-Mère-Enfant, Division of Pediatric Endocrinology, Hospices Civils de Lyon, Lyon 1 University, Lyon, France

<sup>3</sup>INSERM U870, Lyon, France

<sup>4</sup>INSERM CIC201, Lyon, France

<sup>5</sup>INSERM UMR-S958, Faculté de Médecine Paris Diderot, Paris, France

<sup>6</sup>Université Paris Diderot, Sorbonne Paris Cité, Paris, France

<sup>7</sup>Cambridge Institute for Medical Research, University of Cambridge, and National Institute for Health Research Cambridge Biomedical Research Centre, Cambridge, U.K.

<sup>8</sup>Institut de Génétique, Centre National de Génotypage, Commissariat à l'Energie Atomique et aux Energies Alternatives, Evry, France

<sup>9</sup>University of Exeter Medical School, University of Exeter, Exeter, U.K.

<sup>10</sup>Division of Endocrinology, Erasmus Hospital, Brussels, Belgium

Corresponding authors: Marc Nicolino, marc.nicolino@chu-lyon.fr; Miriam Cnop, mcnop@ulb.ac.be; and Cécile Julier, cecile.julier@inserm.fr.

Received 8 April 2015 and accepted 30 June 2015.

This article contains Supplementary Data online at <http://diabetes.diabetesjournals.org/lookup/suppl/doi:10.2337/db15-0477/-/DC1>.

B.A., M.N., M.C., and C.J. contributed equally to this work.

© 2015 by the American Diabetes Association. Readers may use this article as long as the work is properly cited, the use is educational and not for profit, and the work is not altered.

acts under basal conditions (8), while GADD34, encoded by *PPP1R15A*, is activated by eIF2 $\alpha$  phosphorylation and feeds back negatively on PERK signaling to promote the recovery of protein synthesis as the stress response wanes (9). The PERK pathway and its regulation are especially important for pancreatic  $\beta$ -cell function and survival (10–12). Homozygous mutations in *EIF2AK3* cause Wolcott-Rallison syndrome, a syndromic form of neonatal diabetes with epiphyseal dysplasia, growth retardation, and variable other manifestations including microcephaly (11,13)—features mirrored in PerK knockout mice (14). Unmitigated ER stress contributes to  $\beta$ -cell demise in several other monogenic forms of diabetes. Mutations in the insulin gene that disrupt proinsulin folding cause severe  $\beta$ -cell ER stress and neonatal diabetes (15). The loss of the ER cochaperone p58<sup>IPK</sup>, due to *DNAJC3* mutations, leads to a syndrome with young-onset diabetes (16).

Here, we report on a *PPP1R15B* mutation in two siblings with young-onset diabetes, microcephaly, and short stature. The mutation, located in the PP1 binding domain (8), disrupts PP1 binding and eIF2 $\alpha$  dephosphorylation and reveals that  $\beta$ -cell dysfunction and apoptosis may be caused both by too little and by too much eIF2 $\alpha$  phosphorylation.

## RESEARCH DESIGN AND METHODS

### Patients

We studied a consanguineous family of Algerian origin, with two siblings affected by young-onset diabetes that is associated with short stature, microcephaly, and intellectual disability. The study was explained to the patients, their parents, tutors, and other family members, who agreed to participate in the genetic study and signed informed consents. The study protocol was approved by the local ethics committee. Blood samples were obtained from the two affected siblings and two nonaffected relatives (the paternal grandmother and a paternal aunt) and DNA was extracted using standard procedures.

### Exome Sequencing and Analysis

Exome sequencing was performed on the genomic platform of IntegraGen (Evry, France). Exons of genomic DNA of the index case (patient 1) were captured with in-solution enrichment methodology (SureSelect Human All Exon Kits, version 2; Agilent Technologies, Santa Clara, CA) with the company's biotinylated oligonucleotide probe library (Human All Exon, version 2, 50 Mb; Agilent). Genomic DNA was then sequenced on a sequencer as paired-end 75 bases (Illumina HiSeq 2000; Illumina, San Diego, CA). Image analysis and base calling were performed with Real-Time Analysis software, version 1.14 with default parameters (Illumina). Bioinformatic analysis was performed by an in-house pipeline (IntegraGen) based on the Consensus Assessment of Sequence and Variation (CASAVA 1.8; Illumina) to perform alignment against human reference genome (GRCh37/hg19), variant calling, and coverage analysis. The overall sequencing coverage over the whole

exome was 88% and 79% for a 10 $\times$  and 25 $\times$  depth of coverage, respectively, resulting in a mean sequencing depth of 64 $\times$  per base. Exome variant analysis was then performed using an in-house python pipeline on genetic variation annotation results (M.D., A.P., and C.J., unpublished data). Variants were filtered consecutively based on their quality, their genotype (homozygous status), and the predicted consequence on coding capacity (missense, nonsense, splice-site, and coding insertion/deletion—inframe or frameshift) and for their rare status based on information available in in-house (control subjects, IntegraGen) and public databases (Exome Variant Server [EVS], ESP6500SI; Exome Aggregation Consortium [ExAC], release 0.3; and Single Nucleotide Polymorphism database [dbSNP], version 138). Variants that were homozygous or had a minor allele frequency >0.005 in any in-house or public database were excluded.

### Variant Confirmation and Test for Diabetes Segregation in the Family

Each rare variant identified as homozygous in patient 1 by exome sequencing was confirmed in patient 1 and further genotyped in patient 2, in two nonaffected relatives (a paternal grandmother and a paternal aunt), and in an unrelated healthy control subject. This was done by Sanger sequencing or by PCR-restriction fragment length polymorphism (RFLP) genotyping using specific amplification primers and restriction enzymes that differentiate the two alleles, followed by agarose gel electrophoresis using standard techniques. Sequencing primers and PCR-RFLP primers/enzymes are available on request.

### Sanger Sequencing of *PPP1R15B* Exons and Regulatory Regions

Sanger sequencing of *PPP1R15B* exons (coding, 5'UTR and 3'UTR regions) and flanking regions of a 680 base pair of promoter region and a 800 base pair intronic region that shows species conservation and contains unspliced human ESTs (UCSC Genome Browser) was performed by BigDye Terminator sequencing on PCR-amplified DNA using an Applied Biosystems 3730 DNA Sequencer (Foster City, CA). PCR and sequencing primers are shown in Supplementary Table 1. Sequence interpretation was performed using the Genalys software (17).

### Cell Culture

Clonal rat INS-1E cells (a kind gift from Dr. C. Wollheim, Centre Médical Universitaire, Geneva, Switzerland) were cultured in RPMI medium as described (18). Male Wistar rats (Charles River Laboratories, Châtillon-sur-Chalaronne, France) were housed and handled following the rules of the Belgian Regulations for Animal Care. Rat tissues were collected and islets were handpicked under a stereomicroscope after isolation by collagenase digestion (19).  $\beta$ -Cells were purified by autofluorescence-activated cell sorting of dispersed islet cells (FACS, FACSAria; BD Biosciences, Erembodegem, Belgium) and cultured as previously described (20). Human embryonic kidney (HEK)293T cells

were maintained in DMEM supplemented with 10% FBS, 100 mU/mL penicillin, 100 mU/mL streptomycin, and 2 mmol/L L-glutamine.

### Generation of the R658C Mutant PPP1R15B Expression Plasmid

The R658C mutation was introduced in the PPP1R15BpEGFP\_C1 plasmid (21) using QuikChange II Site-Directed Mutagenesis Kit (Agilent) and the primers huPPP1R15B\_R658C\_1S: GTGGTGATGAGGATGCAAAGGACCATGG and huPPP1R15B\_R658C\_2AS: CCATGTCCTTTGCAATCCTCATCACCAC (bold letters indicate the mutation site). This vector allows the expression of recombinant proteins fused to GFP at its N-terminus. After mutagenesis, positive clones were sequenced (Seqlab, Göttingen, Germany), and the following primers were used to cover the entire gene: F1: CATGGTCCTGCTGGAGTTCGTG, F2: AGAGGAGGGGATCCACTG, F3: ACAGTGATGGAAA TAGCGAG, F4: ATCTAGTGAGATACCTATGG, F5: TGA GACCCCTGAGCATAG, Rev: CACACCTCCCCCTGAAC. Plasmids containing the mutation but no other change in the *PPP1R15B* gene were introduced into one-shot TOP10 Electrocomp *Escherichia coli* (Invitrogen, Gent, Belgium) by electroporation. The cells were recovered for 1 h in SOC medium, plated on Luria broth agar containing 50 µg/mL kanamycin, and incubated overnight at 37°C. Selected colonies were grown overnight at 37°C on Luria broth containing 50 µg/mL kanamycin. Plasmids were purified using the PureYield Plasmid Midiprep Kit (Promega, Leiden, the Netherlands) according to the manufacturer's instructions. The DNA concentration was measured using NanoDrop 3300 (Thermo Scientific, Gent, Belgium).

### PPP1R15B Overexpression and Immunoprecipitation

HEK293T cells were transfected with EGFP expression plasmid (pEGFP) without insert (empty vector) or expressing wild type (WT) or mutant PPP1R15B, alone or combined with a mouse PP1A expression plasmid using PEI reagent. After 24 h, the cells were lysed as previously described (8).

Using 1 µL anti-GFP antibody bound to 15 µL protein A sepharose resin, GFP-PPP1R15B was purified from equal amounts of cell lysate protein. The immunoprecipitates containing PPP1R15B were washed twice in lysis buffer before being resolved on a 10% SDS-PAGE gel and blotted onto PVDF (polyvinylidene fluoride) membranes or used for dephosphorylation studies.

### Dephosphorylation Assay

PPP1R15B immunoprecipitates were resuspended in dephosphorylation buffer containing 50 mmol/L Tris (pH 7), 100 mmol/L NaCl, 0.1 mmol/L EDTA, 0.1% Triton X-100, 1 mmol/L DTT, and 1 mmol/L MnCl<sub>2</sub> and incubated with phosphorylated eIF2α for 5–60 min at 30°C. The supernatant was resolved on 15% phos-tagged SDS-PAGE gel and visualized using EZBlue gel staining reagent (Sigma-Aldrich, Dorset, England).

### RNA Interference

Clonal and primary rat β-cells were transfected overnight with 30 nmol/L control small interfering RNA (siRNA) (Qiagen, Germantown, MD) or siRNAs targeting rat PPP1R15B, DP5, PUMA, or Bim using Lipofectamine RNAiMAX (Invitrogen) as previously described (22). The siRNAs used in the current study are listed in Supplementary Table 2.

### Total RNA and mRNA Extraction and Real-Time PCR

Poly(A)<sup>+</sup> mRNA and total RNA were isolated and reverse transcribed as previously described (19,23). Real-time PCR was performed using Rotor-Gene SYBR Green on a Rotor-Gene Q cyclor (Qiagen) (23,24). Primers were used in a conventional PCR for preparing the standards. Gene expression was calculated as copies/µL (25). Expression levels were corrected for expression of the reference gene GAPDH. Primer sequences are provided in Supplementary Table 3.

### Western Blotting

Tissue and cell preparation were performed as previously described (26). Immunoblotting was done using antibodies against β-actin, phosphorylated eIF2α, eIF2α, BCL-2, BCL-XL, caspase 9, caspase 3, Cox IV (Cell Signaling, Leiden, the Netherlands), human α-tubulin (Sigma-Aldrich), human ATF3, human PP1 (Santa Cruz, Heidelberg, Germany), cytochrome c (BD Biosciences), or GFP produced in rabbits. Protein detection was performed using DyLight conjugated secondary antibody or horseradish peroxidase-conjugated secondary antibodies and SuperSignal West Femto chemiluminescence revealing reagent (Thermo Scientific). Immunoreactive bands were detected with a ChemiDoc XRS+ system and with Image Lab software (Bio-Rad, Hercules, CA). Protein levels were corrected for α-tubulin or β-actin.

### Cell Treatment and Apoptosis Assays

Free fatty acid (FFA) exposure was done in RPMI 1640 medium containing 0.75% FFA-free BSA (Roche, Mannheim, Germany) and 1% FBS. Oleate and palmitate (Sigma-Aldrich) were dissolved in 90% ethanol and diluted 1:100 to a final concentration of 0.5 mmol/L (27,28). Cyclopiazonic acid (CPA) was used at 25 µmol/L, tunicamycin at 5 µg/mL, and brefeldin A at 0.1 µg/mL. The PERK inhibitor GSK2606414 was used at 0.5 µmol/L (29). Apoptotic cell death was detected and counted by fluorescence microscopy after Hoechst 33342 (5 µg/mL; Sigma-Aldrich) and propidium iodide (5 µg/mL) staining (28,30).

### Glucose-Stimulated Insulin Secretion

Insulin secretion was measured as previously described (22). Briefly, INS-1E cells were washed with modified Krebs-Ringer bicarbonate HEPES solution (KRB) and incubated for 30 min with KRB without glucose, and insulin secretion was induced by 30-min incubation with KRB containing 1.67 or 16.7 mmol/L glucose with or without 10 µmol/L forskolin. Insulin was measured by ELISA (Mercodia, Uppsala, Sweden) in cell-free supernatants and acid-ethanol extracted cell lysates. Total protein was measured in cell lysates using the Protein Assay Dye Reagent (Bio-Rad).

### Cytochrome C Release

Cells were harvested in PBS 48 h after transfection. After centrifugation, a cytosolic lysis buffer containing 0.8  $\mu\text{g}/\mu\text{L}$  digitonin was added to the pellet. The cells were vortexed for 30 s and centrifuged at 4°C at 20,000 $\times g$  for 1 min. The supernatant was separated as cytoplasmic fraction and the pellet was used as the mitochondrial fraction. Laemmli buffer was added and the samples were resolved on 12% SDS-PAGE.

### Statistical Analysis

Data are presented as means  $\pm$  SE. Given the paired nature of the experimental design, comparisons between groups were made by two-sided Student paired *t* test, with Bonferroni correction for multiple comparisons when needed. A *P* value  $<0.05$  was considered statistically significant.

## RESULTS

### Description of a Novel Diabetes Syndrome With Young-Onset Diabetes, Short Stature, and Microcephaly

We studied two siblings with young-onset diabetes, intellectual disability, microcephaly, and short stature who were born to first-cousin consanguineous parents without diabetes (see Table 1 and Fig. 1 for the description of the patients). The index case (patient 1), a boy, was diagnosed with diabetes at age 15 years, with acute onset of polyuria and polydipsia. Fasting glucose was 13.4 mmol/L and HbA<sub>1c</sub> was 13.0% (119 mmol/mol). Type 1 diabetes-specific auto-antibodies (islet cell antibody, GAD, IA2 antibodies) were negative. Fasting C-peptide was low but within normal range for normoglycemic subjects (Table 1), showing that at least some residual  $\beta$ -cell mass remained. He was treated with twice-daily insulin injections. Diabetes was initially well controlled with relatively low doses of

insulin ( $\sim 0.5$  units/kg/day) but evolved to significant glucose variability with severe hypoglycemia episodes and seizures. He had growth retardation (Fig. 1A), reaching an adult height of 155 cm, with normal growth hormone (peak at 41 ng/mL after ornithine stimulation test; normal reference values [N]  $>10$ ) and IGF1 levels (291  $\mu\text{g}/\text{L}$ ; N = 249–672). Thyroxine (18 pmol/L; N = 10–23) and glucagon (116 ng/L; N = 25–250) levels were normal. Blood cell count, electrolytes, creatinine, liver enzymes, bilirubin, cholesterol, triglycerides, lactate, and pyruvate levels were normal. He had delayed puberty, with an undescended right testis that was surgically corrected. No anomaly of the gonadal function was found, with normal levels of testosterone (9.54 nmol/L; N = 9.0–26.0), luteinizing hormone (4.4 mU/mL; N = 0.24–5.9), and follicle-stimulating hormone (6.5 mU/mL; N = 1.9–11.6). He had microcephaly (adult cranial perimeter: 46 cm,  $-4.0$  SD) and severe intellectual disability, with a quiet introverted character. At 15 years of age, his mental level was comparable to that of a 5- to 6-year-old child. He answered questions using simple sentences but could not read or write. His vocabulary was limited to 200–300 words and he did not engage in conversation. He was able to perform tasks such as feeding, dressing, and bathing but required full assistance in daily life. MRI showed rarefaction of the white matter (Fig. 1B), with a nonspecific slightly elevated level of protein in the cerebrospinal fluid (albumin and IgG). He had neurogenic deafness (hearing loss of 39%). He also had kyphoscoliosis, pectus excavatum, mild abnormalities of vertebral bodies (Fig. 1C and D), fine fingers and toes, oligodontia and dental hypoplasia, sparse hair, and a high-pitched voice. Eye fundus was normal. Clinical and biochemical examination at 28 years of age showed that his diabetes was relatively well controlled (Table 1). Glucagon-stimulated C-peptide was detectable.

**Table 1—Clinical and biochemical characteristics of the two patients**

Sex	Patient 1		Patient 2
	Male		Female
Age at diabetes onset, years	15		28
Age at follow-up examination, years	15*	28	31
Anthropometry			
Height, cm (SD)	146 (−3.5)	155 (−3.2)	139 (−4.2)
Weight, kg (SD)	31.4 (−3.2)	44.3 (−3.5)	30 (−4.0)
BMI, kg/m <sup>2</sup> (SD)	14.7 (−2.7)	18.4 (−1.7)	15.5 (−2.5)
Microcephaly	Yes		Yes
Cranial perimeter, cm (SD)	46 (−4.0)		NA
Glucose metabolism			
HbA <sub>1c</sub> , % [N = 4.0–6.0]	13.0	7.8	NA
C-peptide secretion evaluation			
Fasting glycemia, mmol/L [N = $<5.6$ ]	3.96	11.4	NA
Fasting C-peptide, nmol/L [N = 0.25–1.28]	0.56	NA	NA
Glucagon-stimulated C-peptide, nmol/L [N $>0.6$ ]	NA	0.89	NA
Therapy			
Insulin therapy duration, years	0	13	3
Insulin dose, units/kg/day	0	0.5	0.7

SD is based on French normative values. \*, at diabetes onset.

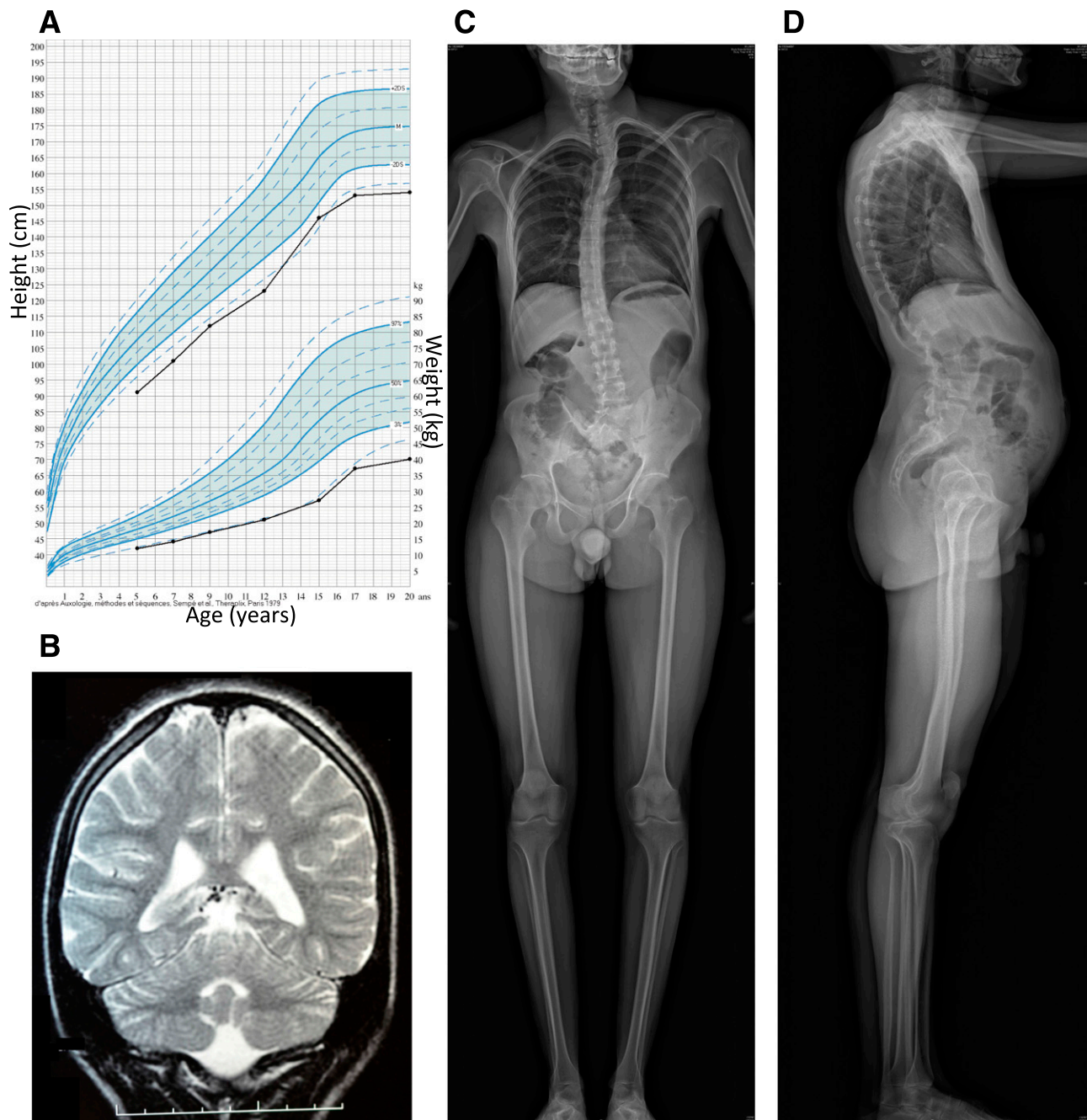


**Figure 1**—Imaging of brain and skeleton of patient 1. **A:** Growth chart, showing growth retardation. **B:** Coronal T2-weighted brain MRI at age 15 years, showing a moderate white matter rarefaction characterized by increased sulcal size and moderate enlargement of ventricular system. **C and D:** Skeletal radiographies at age 28 years, showing kyphoscoliosis with tall vertebral bodies and hyperlordosis.

Pubertal development was fully achieved (Tanner stage 5) with adult genitalia and complete epiphyseal closure on bone age X-ray. Biochemical measurements in serum showed low 25-hydroxyvitamin D (55 nmol/L; N = 75–340), but normal levels of calcium, IGF-1, and thyroxine. Markers of phosphate metabolism were normal: parathyroid hormone (19 pg/mL; N = 10–55), serum phosphate (1.54 mmol/L; N = 1.30–1.85), and alkaline phosphatase (320 units/L; N = 210–830). Urinary calcium-to-creatinine ratio was also normal (0.33; N <0.7). His weight and BMI

were low at 44.3 kg and 18.4 kg/m<sup>2</sup>, respectively. Dual-energy X-ray absorptiometry showed normal body composition and bone mineral content. Overall, these results are in keeping with bone dysplasia without marked disturbance of calcium metabolism, with severe growth retardation unrelated to pituitary or thyroid dysfunction. Serum amylase, blood cell count, liver and kidney function, and iron metabolism were normal. On ultrasound, liver and pancreas were normal, while the kidneys were small, with mild dilation of right calyces.

His sister (patient 2) had a similar clinical presentation, but she was not available for detailed evaluation. She had growth retardation, microcephaly, intellectual disability, and diabetes presenting with an acute onset of hyperglycemia and ketosis at age 28 years. She was treated by insulin. She also had dental hypoplasia, an introverted character, and high-pitched voice. She had menarche at the age of 14 years. At the last examination at 31 years of age, body weight was 30 kg, height 139 cm, BMI 15.5 kg/m<sup>2</sup> (Table 1). Blood cell count, electrolytes, and kidney function parameters were normal. Early clinical history was unavailable for these patients, except for the information that they were born small for gestational age. The parents had normal fasting glucose (father, 5.1 mmol/L; mother, 4.3 mmol/L; N <5.6), and the mother was not known to have had gestational diabetes mellitus. They were unavailable for further clinical examination and genetic study.

#### Identification of a Homozygous Mutation in the *PPP1R15B* Gene in the Two Siblings With Diabetes

Because of the familial context, we hypothesized that the syndrome was caused by an autosomal recessive mutation.

To test this hypothesis, we performed exome sequencing on patient 1's genomic DNA and identified 18 rare homozygous autosomal variants after filtering (coding variants, minor allele frequency <0.005, and absence of subjects homozygous for the rare variant in public and in-house databases; Supplementary Tables 4 and 5). We confirmed these variants in patient 1 and genotyped them in patient 2 and in two nonaffected relatives (a grandmother and an aunt) by Sanger sequencing or PCR-RFLP genotyping. This reduced the number of variants to 6, for which both siblings, but not the unaffected relatives, were homozygous for the rare allele: *ADAMTSL4*, *FLG*, *KIF21B*, *PPP1R15B*, and *SLC45A3*, located on chromosome 1, and *UNC80*, located on chromosome 2 (Supplementary Tables 5 and 6). Because of the relative similarities of this syndrome with Wolcott-Rallison syndrome (*EIF2AK3* mutations), the features of the *Ppp1r15b*<sup>-/-</sup> mouse (very small size at birth and early death), and its role in the ER stress response (31), *PPP1R15B* (Fig. 2A) appeared as the major candidate (Supplementary Table 6). None of the other genes showed obvious functional relevance to the syndrome (Supplementary Table 6). *PPP1R15B* is ubiquitously expressed (and well

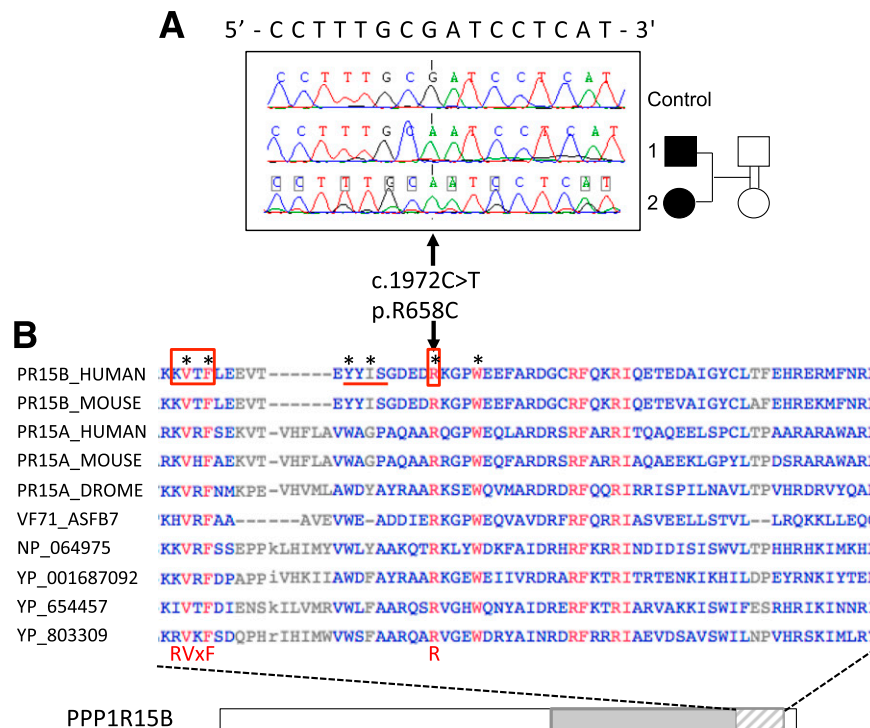


**Figure 2**—Identification of a homozygous *PPP1R15B*-R658C mutation in two siblings with diabetes and consequences of the mutation on the protein. **A**: Sanger sequencing of a control subject and the two siblings with diabetes (filled symbols), presenting the homozygous mutation and its consequence on the cDNA and protein. **B**: *PPP1R15B* protein sequence, showing the alignment of a highly conserved 62 amino acid segment (hatched) located within the COOH-terminal functional core region (gray). Representative sequences aligned are *PPP1R15B* from human (PR15B\_HUMAN, Q5SWA1) and mouse (PR15B\_MOUSE, Q8BFW3); *PPP1R15A* from human (PR15A\_HUMAN, O75807), mouse (PR15A\_MOUSE, P17564), and drosophila (PR15A\_DROME, Q9W1E4); and homologous proteins from a variety of viruses: African Swine fever virus (VF71\_ASFB7, Q65212), Amsacta moorei entomopoxvirus L (NP\_064975), Glossina pallidipes salivary gland hypertrophy virus (YP\_001687092), Choristoneura occidentalis granulovirus (YP\_654457), and Trichoplusia ni ascovirus 2c (YP\_803309). The mutated arginine (R) at position 658 is part of the functional RVxF-ΦΦ-R motif (boxed and underlined on human *PPP1R15B*) that has been recognized in PP1-interacting proteins (33). Residues shown in red are fully conserved in selected species; residues that are the most critical for establishing contact with PP1 according to Chen et al. (32) are indicated by stars.

expressed in human islets and  $\beta$ -cells), consistent with the multisystem disease manifestations, while the other genes have a lower expression in islets and their pattern of tissue expression does not specifically correspond to the syndrome (Supplementary Fig. 1, Supplementary Table 6). The R658 residue of *PPP1R15B* is highly conserved between organisms, including viruses (Fig. 2B), and the R658C mutation is predicted to be damaging by in silico prediction programs (Supplementary Table 6). It is located in the conserved COOH-terminal functional core of PPP1R15B that specifies interaction with PP1, the recruitment of the essential cofactor G-actin, and substrate-specific dephosphorylation (21,32). In the cocrystal structure, PPP1R15B R658 inserts deep into a pocket on the surface of PP1 (34), giving rise to an ionic interaction with PP1 residue D71 that is conserved in other holophosphatases such as PP1-PPP1R10 (PNUTS) and PP1-PPP1R9B (spinophilin) (33). Collectively, these structural observations strongly support a critical role of R658 in PP1 binding and predict that the mutation of this residue has deleterious effects on protein function.

To search for additional patients with *PPP1R15B* mutations, we performed Sanger sequencing of *PPP1R15B* exons, flanking regions, and main regulatory regions (Supplementary Table 1) in 50 patients with a similar clinical

presentation, i.e., insulin-dependent diabetes and short stature and/or mental retardation or microcephaly, and in 22 patients with diabetes and their families compatible with monogenic diabetes and linkage to the *PPP1R15B* chromosome region (C.J., unpublished data), but we did not identify any homozygous or compound heterozygous *PPP1R15B* mutations in these patients.

### R658C Mutation Destabilizes the PPP1R15B-PP1 Complex and Impairs eIF2 $\alpha$ Dephosphorylation

To study the effect of the R658C mutation on PPP1R15B function, we generated a plasmid encoding the fusion of WT or R658C-mutated human PPP1R15B to EGFP. HEK293T cells were transfected with either plasmid or the empty pEGFP vector, alone or in combination with a plasmid expressing mouse PP1A. The PPP1R15B-PP1 complex was immunoprecipitated from cell lysates using anti-GFP antibody and analyzed for the presence of PP1 by Western blot. Fewer PP1 were recovered in complex with mutant PPP1R15B-EGFP compared with WT. This was true both when endogenous PP1 was examined (compare lanes 1 and 2, Fig. 3A) and when PP1A was overexpressed (compare lanes 5 and 6, Fig. 3A), demonstrating that the R658C mutation reduced the ability of PPP1R15B to bind PP1, as suggested by the structural studies.

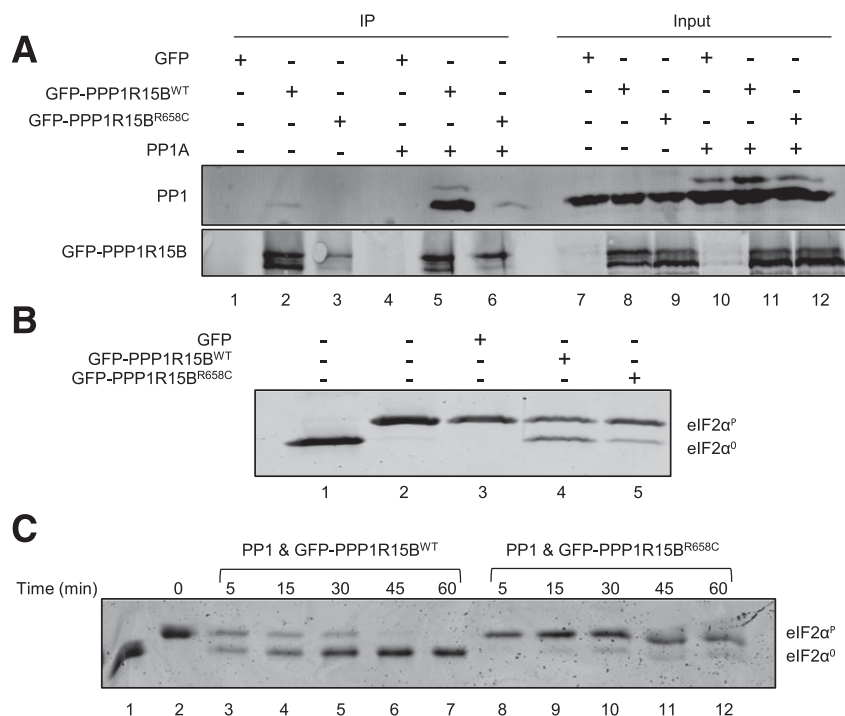


**Figure 3**—The R658C mutation destabilizes the PPP1R15B-PP1 complex and diminishes its phosphatase activity. HEK293T cells were transfected with an empty vector (GFP) or a GFP-tagged WT or R658C-mutated human PPP1R15B, alone or in combination with a mouse PP1A expression plasmid. PPP1R15B-PP1 complexes were immunoprecipitated from lysed cells with anti-GFP antibody. **A**: The recovery of PP1 in complex with PPP1R15B was examined by Western blotting using anti-PP1 antibody. Immunoprecipitated protein is shown on the left (IP) and the eluant is shown on the right (input). **B**: The holophosphatase activity was studied in an eIF2 $\alpha$  dephosphorylation assay, incubating the indicated PPP1R15B-PP1 complexes purified from cells with in vitro phosphorylated eIF2 $\alpha$  (eIF2 $\alpha^p$ ) protein for 30 min and resolving the phosphorylated and nonphosphorylated eIF2 $\alpha$  (eIF2 $\alpha^o$ ) on Phos-tag gels. **C**: A time course of eIF2 $\alpha$  dephosphorylation by WT and R658C-mutated PPP1R15B and PP1A complexes recovered by immunopurification from transfected HEK293T cells. Unphosphorylated eIF2 $\alpha$  was loaded onto lane 1 as a reference. The blots are representative of three or more independent experiments with similar outcomes.

Next, we examined the dephosphorylation activity of the immunopurified PPP1R15B-PP1 holophosphatase complex. Complexes recovered by immunopurification of GFP-tagged WT PPP1R15B were more active at dephosphorylating eIF2 $\alpha$  in vitro than complexes constituted of the R658C mutant (compare lanes 4 and 5, Fig. 3B). These differences were rendered more conspicuous in a time course study. Complexes containing WT PPP1R15B substantially dephosphorylated eIF2 $\alpha$  protein by 45 min, whereas in dephosphorylation reactions carried out with R658C mutant PPP1R15B, substantial amounts of phosphorylated eIF2 $\alpha$  remained even at the 60-min time

point (compare lanes 7 and 12, Fig. 3C). Thus, the missense mutation R658C negatively affects the stability of the PPP1R15B-PP1 complex and, in turn, its ability to dephosphorylate eIF2 $\alpha$ .

#### PPP1R15B Expression in $\beta$ -Cells

In clonal rat INS-1E  $\beta$ -cells, PPP1R15B was induced by different synthetic ER stressors and the saturated FFA palmitate (Fig. 4A). This induction was prevented by a chemical inhibitor of PERK (Fig. 4B), suggesting that, different from other cell types (8), PPP1R15B expression in  $\beta$ -cells is controlled by the UPR.

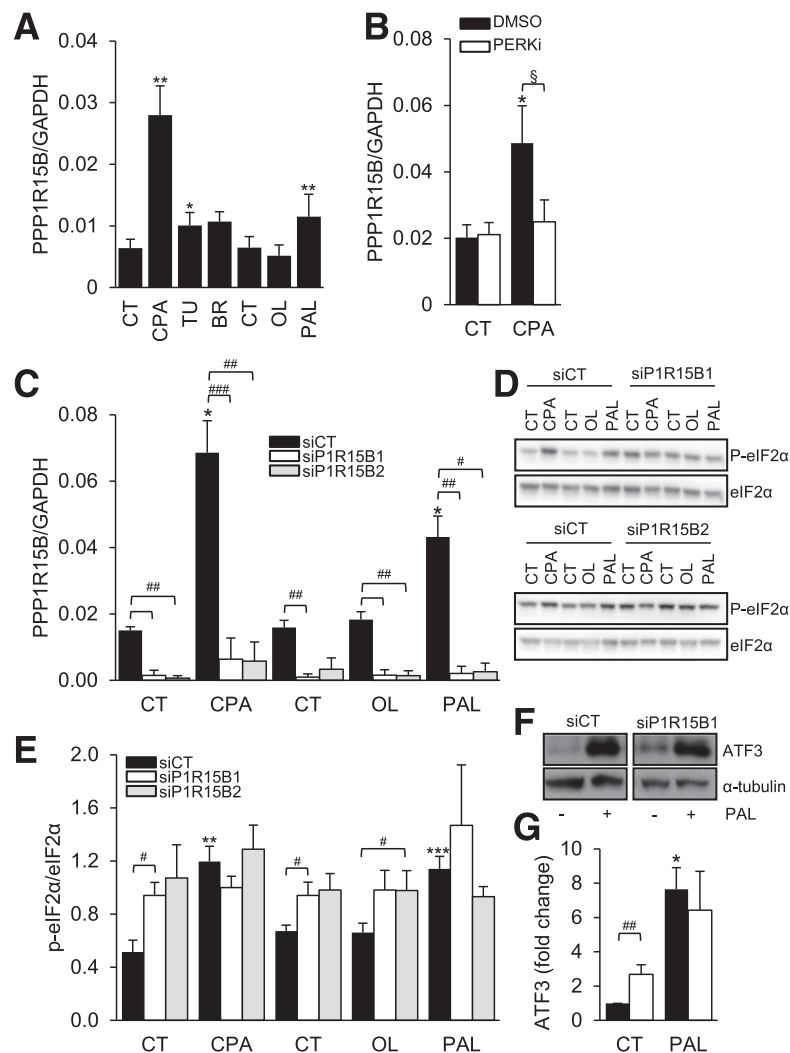


**Figure 4**—PPP1R15B is induced by ER stress in  $\beta$ -cells in a PERK-dependent manner, and PPP1R15B silencing induces eIF2 $\alpha$  phosphorylation and ATF3 in  $\beta$ -cells. **A:** INS-1E cells were exposed to the chemical ER stressors CPA, tunicamycin (TU), or brefeldin A (BR) or to the FFAs oleate (OL) or palmitate (PAL) for 24 h ( $n = 5-6$ ). **B:** INS-1E cells were exposed or not (CT) to CPA in the presence or absence of the PERK inhibitor GSK2606414 (PERKi). PPP1R15B mRNA expression was examined by real-time PCR and normalized to the reference gene GAPDH. **C:** INS-1E cells were transfected with control siRNA (siCT) or two different siRNAs targeting PPP1R15B (P1R15B1 and P1R15B2). After a 48-h transfection, the cells were treated for 16 h with CPA, OL, or PAL. PPP1R15B mRNA expression was examined by real-time PCR and normalized to the reference gene GAPDH ( $n = 4$ ). eIF2 $\alpha$  phosphorylation (P-eIF2 $\alpha$ ) (**D** and **E**) and ATF3 (**F** and **G**) expression were examined by Western blot. **D** and **F** are representative images of  $n = 4$ . **E** and **G** represent densitometric quantifications of **D** and **F**, respectively. P-eIF2 $\alpha$  was corrected for total eIF2 $\alpha$ . ATF3 expression was corrected for  $\alpha$ -tubulin and expressed as fold of CT. Data are presented as means  $\pm$  SE. \*treated vs. control, §DMSO vs. PERKi, #siP1R15B vs. siCT by two-sided Student paired *t* test. \*, §, # $P < 0.05$ ; \*\*, ### $P < 0.01$ ; \*\*\*, #### $P < 0.001$ .

### PPP1R15B Deficiency Increases eIF2 $\alpha$ Phosphorylation in $\beta$ -Cells

Using RNA interference, PPP1R15B was knocked down in INS-1E cells, resulting in a 75% inhibition of mRNA expression (Fig. 4C). Consistent with its previously reported function of constitutive eIF2 $\alpha$  phosphatase (8), basal eIF2 $\alpha$  phosphorylation was increased in PPP1R15B-deficient INS-1E cells (Fig. 4D and E). PPP1R15B silencing did not further increase eIF2 $\alpha$  phosphorylation induced by the synthetic ER stressor CPA or palmitate (Fig. 4D and E). Phosphorylated eIF2 $\alpha$  levels were higher in PPP1R15B-deficient cells exposed to the unsaturated FFA oleate that per se does not induce eIF2 $\alpha$  phosphorylation (28,34). ATF3 protein was also induced in PPP1R15B-deficient cells under basal conditions (Fig. 4F and G). Thus, PPP1R15B silencing increases eIF2 $\alpha$  phosphorylation and induces downstream ATF3 protein expression.

### PPP1R15B Silencing Decreases Insulin Content and Glucose-Stimulated Insulin Release

We next evaluated the effect of PPP1R15B deficiency on  $\beta$ -cell function. PPP1R15B knockdown decreased insulin content in INS-1E cells by 20% (Fig. 5A). In control siRNA-transfected  $\beta$ -cells, high glucose exposure (16.7 mmol/L) increased insulin secretion by 2.8-fold. PPP1R15B-deficient  $\beta$ -cells showed increased basal insulin secretion and little or no response to high glucose (Fig. 5B). 16.7 mmol/L glucose plus forskolin induced insulin secretion by 10-fold in control siRNA-transfected cells, but only by fourfold after PPP1R15B silencing ( $P < 0.05$ ).

### PPP1R15B-Deficient $\beta$ -Cells Are Sensitized to Apoptosis Through the Proapoptotic BH3-Only Proteins DP5, PUMA, and Bim

We examined the role of PPP1R15B in  $\beta$ -cell survival. PPP1R15B silencing in clonal (Fig. 6A and B) and primary

rat  $\beta$ -cells (Fig. 6C) sensitized the cells to apoptosis under basal conditions and induced up to 20% more apoptosis following exposure to CPA or the FFAs oleate and palmitate (Fig. 6A–C).

To evaluate whether the intrinsic pathway of apoptosis was involved, we measured mitochondrial cytochrome c release to the cytoplasm and cleavage of caspase-9 and -3. In PPP1R15B-deficient INS-1E cells, cytoplasmic cytochrome c levels were increased (Fig. 6D) and caspase-9 (Fig. 6E) and -3 (Fig. 6F) were cleaved, demonstrating activation of the intrinsic pathway of apoptosis.

We next examined which BCL-2 family members activate the intrinsic pathway of apoptosis. PPP1R15B deficiency induced mRNA expression of the proapoptotic proteins DP5 and PUMA (Fig. 6G and H), but it did not significantly affect expression of Bim-S protein (Fig. 6I). The expression of Bim-L and EL (Supplementary Fig. 2A–C) and the antiapoptotic proteins BCL-2 and BCL-XL (Supplementary Fig. 2D–F) were not modified by PPP1R15B deficiency. DP5, PUMA, or Bim silencing partially protected PPP1R15B-silenced  $\beta$ -cells from apoptosis (Fig. 6J), showing that PPP1R15B deficiency induces apoptosis through the proapoptotic BH3-only proteins DP5, PUMA, and Bim.

## DISCUSSION

R658C is the first reported mutation in *PPP1R15B*, responsible for a novel diabetes syndrome with onset in youth/young adulthood. It affects a key amino acid in the conserved C-terminus region of the protein that makes contacts with PP1 that is conserved in other holophosphatase complexes (32,33). We show that the R658C mutation destabilizes the complex between PPP1R15B and PP1, and this, in turn, diminishes eIF2 $\alpha$  dephosphorylation. Furthermore, we show that PPP1R15B silencing alters  $\beta$ -cell function, inducing higher basal insulin secretion and reducing high glucose responsiveness, which is compatible with a role of PPP1R15B in exocytosis (35). This is consistent with the observation of residual C-peptide in the index patient and his moderate insulin requirement and frequent hypoglycemic events. PPP1R15B silencing also sensitizes  $\beta$ -cells to apoptosis, both under basal and ER stress conditions, which was induced via the intrinsic pathway of apoptosis, as in the case of palmitate-induced eIF2 $\alpha$  phosphorylation (36).

Of note, diabetes manifested relatively late in these patients (at ages 15 and 28 years). Considering the congenital nature of the defect, this suggests the role of compensatory mechanisms that maintain a sufficient  $\beta$ -cell function for several years. The acute onset of diabetes suggests a threshold mechanism(s) by which this delicate balance is disrupted at some stage, as observed in autoimmune type 1 diabetes and other forms of monogenic diabetes, leading to hyperglycemia (37).

The syndrome caused by the PPP1R15B-R658C mutation results in multisystem manifestations, affecting  $\beta$ -cells (diabetes), the nervous system (microcephaly,

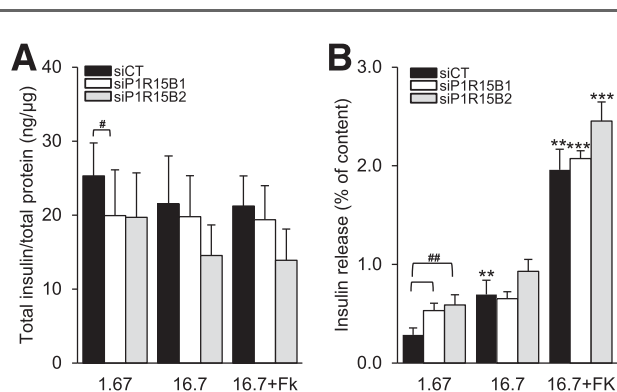


**Figure 5**—Glucose-stimulated insulin secretion is blunted by PPP1R15B deficiency in  $\beta$ -cells. INS-1E cells were transfected with control siRNA (siCT) or two siRNAs targeting PPP1R15B (siP1R15B1 and siP1R15B2). After a 48-h transfection, insulin secretion was induced by 1.67 mmol/L or 16.7 mmol/L glucose or 16.7 mmol/L glucose + 10  $\mu$ mol/L forskolin (16.7+FK). A: Cellular insulin content corrected for total protein. B: Insulin release as percent of insulin content ( $n = 5$ ). \*\* $P < 0.01$ , \*\*\* $P < 0.001$  vs. 1.67 mmol/L glucose. # $P < 0.05$ , ## $P < 0.01$ , siP1R15B vs. siCT.

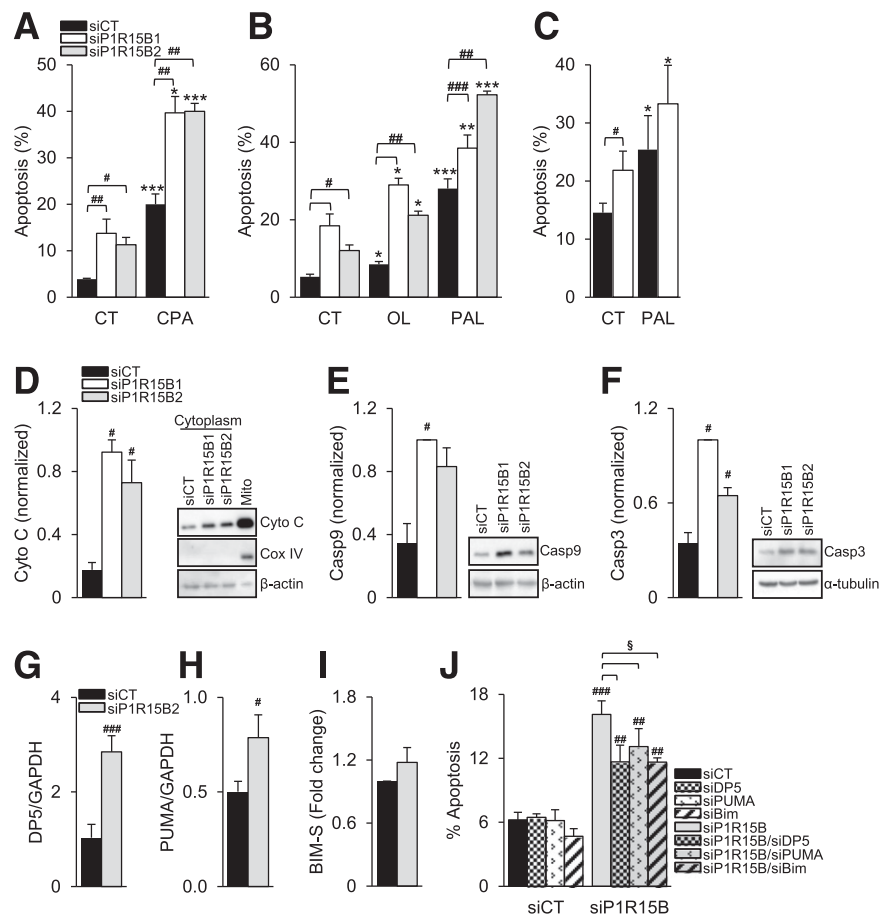


**Figure 6**—PPP1R15B deficiency sensitizes  $\beta$ -cells to FFA- and ER stress-induced apoptosis and activates the intrinsic pathway of apoptosis via DP5, PUMA, and Bim-S. INS-1E (A and B) or primary rat  $\beta$ -cells (C) were transfected with a control siRNA (siCT) or two different siRNAs targeting PPP1R15B (siP1R15B1 and siP1R15B2). After a 24-h transfection, the cells were exposed or not (CT) to CPA, oleate (OL), or palmitate (PAL) for 16 (A and B) or 24 h (C) ( $n = 4$ –5). D: Mitochondrial cytochrome c (Cyto C) release was detected by Western blot in the cytoplasmic fraction 48 h after PPP1R15B knockdown. The right lane shows a noncytoplasmic fraction that includes mitochondria (Mito). Cox IV was used as a mitochondrial control and  $\beta$ -actin as a cytoplasmic control. Activation of caspase-9 (Casp9) (E) and caspase-3 (Casp3) (F) was detected by Western blot 48 h after PPP1R15B knockdown.  $\beta$ -Actin and  $\alpha$ -tubulin were used as loading controls. D, E, and F are representative blots of 4–5 experiments. The densitometry data were normalized to the highest value. DP5 (G) and PUMA (H) mRNA expression were measured by real-time PCR and corrected for the reference gene GAPDH ( $n = 4$ ). Bim-S levels were measured by Western blot (Supplementary Fig. 2), corrected for  $\alpha$ -tubulin, and expressed as fold of siCT (I) ( $n = 5$ ). J: PPP1R15B was silenced alone or in combination with DP5, PUMA, or Bim, and apoptosis was examined by Hoechst 33342/propidium iodide staining ( $n = 3$ –4). \* $P < 0.05$ , \*\* $P < 0.01$ , \*\*\* $P < 0.001$ , treated vs. control. # $P < 0.05$ , ## $P < 0.01$ , ### $P < 0.001$ , siP1R15B vs. siCT. § $P < 0.05$ , single vs. double knockdown.

intellectual disability, and hearing loss), and bone (bone deformities) and general development. This phenotypic spectrum has interesting overlap with other mutations affecting the levels of ER stress or the response to it. Hence,  $\beta$ -cell dysfunction, bone abnormalities, microcephaly, and intellectual disability are shared with the Wolcott-Rallison syndrome caused by *EIF2AK3* mutations, which lead to higher levels of ER stress associated with less eIF2 $\alpha$  phosphorylation (11,13,38), and with syndromes caused by mutations in the ER cochaperone *DNAJC3* and in the immediate early response 3 interacting protein 1 (*IER3IP1*), which both lead to higher levels of ER stress with more eIF2 $\alpha$  phosphorylation (16,39,40). These commonalities likely reflect the importance of balanced ER protein synthesis and folding to the function of

secretory cells, with insulin-producing  $\beta$ -cells, collagen-producing bone cells, and nerve cells especially vulnerable to imbalance. In the Wolcott-Rallison syndrome (with decreased eIF2 $\alpha$  phosphorylation), neonatal diabetes is due to  $\beta$ -cell loss and C-peptide is undetectable (13), while *DNAJC3*, *IER3IP1*, and *PPP1R15B* mutations (with increased eIF2 $\alpha$  phosphorylation) lead to permanent neonatal or young-onset diabetes with residual C-peptide levels, as reported by Synofzik et al. (16), Shalev et al. (40), and the current study. It is notable that the mutations affecting the target of phosphorylated eIF2 $\alpha$ , the guanine nucleotide exchange factor eIF2B, feature prominent neurodegenerative manifestations known as the CACH (childhood ataxia with central nervous system hypomyelination)/VWM (vanishing white matter disease)

syndrome (41), which are phenocopied by targeted activation of the eIF2 $\alpha$  kinase PERK in the brain (42). Interestingly, severe forms of CACH/VWM also have multiorgan manifestations (41,43). The clinical variability of syndromes associated with dysregulated eIF2 $\alpha$  phosphorylation likely results from the interplay of several factors, including the extent of apoptosis and/or secretory dysfunction resulting from specific genes mutations, the severity of the mutation, and possibly environmental stresses.

The clinical features of *PPP1R15B*-mutated patients described here and the phenotype of knockout mice that we described previously (31) suggest that *PPP1R15B* deficiency affects multiple cell types. The role of *PPP1R15B* in exocytosis and membrane traffic has been previously reported in human epithelial cells and erythroleukemia cells (35). The knockdown of *PPP1R15B* in breast cancer cells resulted in impaired cell cycle transition from G1 to S phase and apoptosis (44). These observations suggest that *PPP1R15B* regulates a variety of functions in different cell types. More studies are needed to explore this further.

Although we selected *PPP1R15B* as an obvious candidate gene and found ample structural and functional experimental support for the impact of the mutation, we cannot formally exclude that one of the rare variants homozygous in the two affected siblings contributes to the syndrome. This hypothesis is unlikely based on the following reasons (Supplementary Table 6 and Supplementary Fig. 1): 1) none of the other genes appear directly functionally relevant to the clinical presentation; 2) the expression pattern of *PPP1R15B*, but not of the five other genes, is consistent with the multisystem presentation of the syndrome; 3) mutations in *ADAMTSL4* cause ectopia lentis and mutations in *FLG* cause atopic dermatitis and ichthyosis vulgaris, and none of these diseases were present in the two affected siblings; and 4) human or mouse disease phenotypes of *KIF21B*, *SLC45A3*, and *UNC80* mutations have not been reported so far, and a cellular phenotype of chromosome instability has been reported in *Kif21b*<sup>-/-</sup> mice, which was not observed in our patients. In short, the characteristics of these five other genes show little relevance to the diabetes and neurological phenotype of our patients.

The present human genetic observations are in keeping with our earlier findings that excessive eIF2 $\alpha$  phosphorylation is poorly tolerated by  $\beta$ -cells. Salubrinal, a chemical inhibitor of eIF2 $\alpha$  dephosphorylation, was identified in a large-scale chemical screening as a compound that protects from ER stress (45), and it was even suggested as a potential therapy to preserve  $\beta$ -cells in diabetes (46). In rodent and human  $\beta$ -cells, however, salubrinal actually exacerbates cell death through ER stress and downstream activation of the mitochondrial pathway of apoptosis (10,24). The present observations support the concept that dysregulation of eIF2 $\alpha$  phosphorylation, either excessive (*PPP1R15B*, *DNAJC3*, and *IER3IP1* mutations) or diminished (*EIF2AK3* mutations), is detrimental to  $\beta$ -cells,

neurons, and bone and suggest that other proteins involved in the regulation of protein translation may lead to similar diabetes syndromes.

**Acknowledgments.** The authors are very grateful to the patients and their family for their participation in the study. The authors thank Christophe Caloustian and Sylvana Pavek from the Centre National de Génotypage for expert technical assistance. The authors are also grateful to the Flow Cytometry Facility of the Erasmus Campus of the Université Libre de Bruxelles and Christine Dubois for the cell sorting. The authors thank Michael Pangerl, Anyishai Musuaya, Nathalie Pachera, Stephanie Mertens, and Isabelle Millard at the ULB Center for Diabetes Research (Université Libre de Bruxelles) for excellent technical support. The authors also thank Annabelle Chaussonot from the School of Medicine, Nice Sophia Antipolis University, for contributing some patients for this study and for interesting discussions. The authors thank Dr. Belkacem Bioud, University Hospital of Setif, Algeria, and Dr. Hadda Baaziz, University Hospital of Batna, Algeria, for their collaboration.

**Funding.** This work was supported by the European Union 7th Framework Programme (project BetaBat), the Actions de Recherche Concertées de la Communauté Française, and Fonds National de la Recherche Scientifique (FNRS), Belgium, and by grants from the Agence Nationale pour la Recherche (ANR-09-GENO-021), the European Foundation for the Study of Diabetes/JDRF/Novo Nordisk, the Assistance Publique-Hôpitaux de Paris Programme Hospitalier de Recherche Clinique (DIAGENE), the GIS Maladies Rares, and the Wellcome Trust (084812/Z/08/Z). A.T.H. is a Wellcome Trust and National Institute for Health Research senior investigator, and D.R. is a Wellcome Trust Principal Research Fellow. B.A. was supported by an European Molecular Biology Organization Short-Term Fellowship and an FNRS-FRIA fellowship. M.I.-E. is a scientific collaborator of the FNRS. M.D. was supported by a doctoral fellowship from the Ministère de l'Éducation Nationale, de l'Enseignement Supérieur et de la Recherche, France.

**Duality of Interest.** No potential conflicts of interest relevant to this article were reported.

**Author Contributions.** B.A., M.N., A.P., D.L.E., D.R., M.C., and C.J. contributed to the study design. M.D., S.R., A.P., V.S., C.D., and C.J. performed the genetic experiments and analyzed and interpreted the genetic data. B.A., M.I.-E., M.L., D.A.C., H.P.H., D.L.E., D.R., and M.C. performed the functional experiments and analyzed and interpreted the functional data. M.N. and N.B. identified the index patient and family and characterized these patients. M.N., N.B., and A.T.H. contributed patients. B.A., M.N., A.P., D.R., M.C., and C.J. wrote the manuscript. All coauthors read and approved the manuscript. C.J. is the guarantor of this work and, as such, had full access to all the data in the study and takes responsibility for the integrity of the data and the accuracy of the data analysis.

**Prior Presentation.** Parts of this study were presented in abstract form at the 51st European Association for the Study of Diabetes Annual Meeting, Stockholm, Sweden, 14–18 September 2015.

## References

- Eizirik DL, Cardozo AK, Cnop M. The role for endoplasmic reticulum stress in diabetes mellitus. *Endocr Rev* 2008;29:42–61
- Cnop M, Fougère F, Velloso LA. Endoplasmic reticulum stress, obesity and diabetes. *Trends Mol Med* 2012;18:59–68
- Marhfour I, Lopez XM, Lefkaiditis D, et al. Expression of endoplasmic reticulum stress markers in the islets of patients with type 1 diabetes. *Diabetologia* 2012;55:2417–2420
- Laybutt DR, Hawkins YC, Lock J, et al. Influence of diabetes on the loss of beta cell differentiation after islet transplantation in rats. *Diabetologia* 2007;50:2117–2125
- Marchetti P, Bugliani M, Lupi R, et al. The endoplasmic reticulum in pancreatic beta cells of type 2 diabetes patients. *Diabetologia* 2007;50:2486–2494

6. Hartman MG, Lu D, Kim ML, et al. Role for activating transcription factor 3 in stress-induced beta-cell apoptosis. *Mol Cell Biol* 2004;24:5721–5732
7. Ron D, Walter P. Signal integration in the endoplasmic reticulum unfolded protein response. *Nat Rev Mol Cell Biol* 2007;8:519–529
8. Jousse C, Oyadomari S, Novoa I, et al. Inhibition of a constitutive translation initiation factor 2 $\alpha$  phosphatase, CREP, promotes survival of stressed cells. *J Cell Biol* 2003;163:767–775
9. Novoa I, Zeng H, Harding HP, Ron D. Feedback inhibition of the unfolded protein response by GADD34-mediated dephosphorylation of eIF2 $\alpha$ . *J Cell Biol* 2001;153:1011–1022
10. Cnop M, Ladrère L, Hekerman P, et al. Selective inhibition of eukaryotic translation initiation factor 2 alpha dephosphorylation potentiates fatty acid-induced endoplasmic reticulum stress and causes pancreatic beta-cell dysfunction and apoptosis. *J Biol Chem* 2007;282:3989–3997
11. Delépine M, Nicolino M, Barrett T, Golamaully M, Lathrop GM, Julier C. EIF2AK3, encoding translation initiation factor 2-alpha kinase 3, is mutated in patients with Wolcott-Rallison syndrome. *Nat Genet* 2000;25:406–409
12. Scheuner D, Song B, McEwen E, et al. Translational control is required for the unfolded protein response and in vivo glucose homeostasis. *Mol Cell* 2001;7:1165–1176
13. Julier C, Nicolino M. Wolcott-Rallison syndrome. *Orphanet J Rare Dis* 2010;5:29
14. Harding HP, Zeng H, Zhang Y, et al. Diabetes mellitus and exocrine pancreatic dysfunction in *perk*<sup>-/-</sup> mice reveals a role for translational control in secretory cell survival. *Mol Cell* 2001;7:1153–1163
15. Støy J, Edghill EL, Flanagan SE, et al.; Neonatal Diabetes International Collaborative Group. Insulin gene mutations as a cause of permanent neonatal diabetes. *Proc Natl Acad Sci U S A* 2007;104:15040–15044
16. Synofzik M, Haack TB, Kopajtic R, et al. Absence of BiP co-chaperone DNAJC3 causes diabetes mellitus and multisystemic neurodegeneration. *Am J Hum Genet* 2014;95:689–697
17. Takahashi M, Matsuda F, Margetic N, Lathrop M. Automated identification of single nucleotide polymorphisms from sequencing data. *J Bioinform Comput Biol* 2003;1:253–265
18. Ortis F, Cardozo AK, Crispim D, Störling J, Mandrup-Poulsen T, Eizirik DL. Cytokine-induced proapoptotic gene expression in insulin-producing cells is related to rapid, sustained, and nonoscillatory nuclear factor-kappaB activation. *Mol Endocrinol* 2006;20:1867–1879
19. Rasschaert J, Ladrère L, Urbain M, et al. Toll-like receptor 3 and STAT-1 contribute to double-stranded RNA+ interferon- $\gamma$ -induced apoptosis in primary pancreatic  $\beta$ -cells. *J Biol Chem* 2005;280:33984–33991
20. Marroqui L, Masini M, Merino B, et al. Pancreatic  $\alpha$  cells are resistant to metabolic stress-induced apoptosis in type 2 diabetes. *EBioMedicine* 2015;2:378–385
21. Chambers JE, Dalton LE, Clarke HJ, et al. Actin dynamics tune the integrated stress response by regulating eukaryotic translation initiation factor 2 $\alpha$  dephosphorylation. *eLife* 2015;4:e04872
22. Cnop M, Igoillo-Esteve M, Rai M, et al. Central role and mechanisms of  $\beta$ -cell dysfunction and death in friedreich ataxia-associated diabetes. *Ann Neurol* 2012;72:971–982
23. Kharroubi I, Ladrère L, Cardozo AK, Dogusan Z, Cnop M, Eizirik DL. Free fatty acids and cytokines induce pancreatic  $\beta$ -cell apoptosis by different mechanisms: role of nuclear factor-kappaB and endoplasmic reticulum stress. *Endocrinology* 2004;145:5087–5096
24. Ladrère L, Igoillo-Esteve M, Cunha DA, et al. Enhanced signaling downstream of ribonucleic acid-activated protein kinase-like endoplasmic reticulum kinase potentiates lipotoxic endoplasmic reticulum stress in human islets. *J Clin Endocrinol Metab* 2010;95:1442–1449
25. Overbergh L, Valckx D, Waer M, Mathieu C. Quantification of murine cytokine mRNAs using real time quantitative reverse transcriptase PCR. *Cytokine* 1999;11:305–312
26. Moore F, Colli ML, Cnop M, et al. PTPN2, a candidate gene for type 1 diabetes, modulates interferon- $\gamma$ -induced pancreatic  $\beta$ -cell apoptosis. *Diabetes* 2009;58:1283–1291
27. Cnop M, Hannaert JC, Hoorens A, Eizirik DL, Pipeleers DG. Inverse relationship between cytotoxicity of free fatty acids in pancreatic islet cells and cellular triglyceride accumulation. *Diabetes* 2001;50:1771–1777
28. Cunha DA, Hekerman P, Ladrère L, et al. Initiation and execution of lipotoxic ER stress in pancreatic  $\beta$ -cells. *J Cell Sci* 2008;121:2308–2318
29. Harding HP, Zyryanova AF, Ron D. Uncoupling proteostasis and development in vitro with a small molecule inhibitor of the pancreatic endoplasmic reticulum kinase, PERK. *J Biol Chem* 2012;287:44338–44344
30. Igoillo-Esteve M, Marselli L, Cunha DA, et al. Palmitate induces a pro-inflammatory response in human pancreatic islets that mimics CCL2 expression by beta cells in type 2 diabetes. *Diabetologia* 2010;53:1395–1405
31. Harding HP, Zhang Y, Scheuner D, Chen JJ, Kaufman RJ, Ron D. Ppp1r15 gene knockout reveals an essential role for translation initiation factor 2 alpha (eIF2 $\alpha$ ) dephosphorylation in mammalian development. *Proc Natl Acad Sci U S A* 2009;106:1832–1837
32. Chen R, Rato C, Yan Y, et al. G-actin provides substrate-specificity to eukaryotic translation initiation factor 2 $\alpha$  holophosphatases. *eLife* 2015;4:e04871
33. Choy MS, Hieke M, Kumar GS, et al. Understanding the antagonism of retinoblastoma protein dephosphorylation by PNU19752 provides insights into the PP1 regulatory code. *Proc Natl Acad Sci U S A* 2014;111:4097–4102
34. Karaskov E, Scott C, Zhang L, Teodoro T, Ravazzola M, Volchuk A. Chronic palmitate but not oleate exposure induces endoplasmic reticulum stress, which may contribute to INS-1 pancreatic  $\beta$ -cell apoptosis. *Endocrinology* 2006;147:3398–3407
35. Kloft N, Neukirch C, von Hoven G, et al. A subunit of eukaryotic translation initiation factor 2 $\alpha$ -phosphatase (CreP/PPP1R15B) regulates membrane traffic. *J Biol Chem* 2012;287:35299–35317
36. Cunha DA, Igoillo-Esteve M, Gurzov EN, et al. Death protein 5 and p53-upregulated modulator of apoptosis mediate the endoplasmic reticulum stress-mitochondrial dialog triggering lipotoxic rodent and human  $\beta$ -cell apoptosis. *Diabetes* 2012;61:2763–2775
37. Eizirik DL, Sandler S, Palmer JP. Repair of pancreatic beta-cells. A relevant phenomenon in early IDDM? *Diabetes* 1993;42:1383–1391
38. de Wit MC, de Coo IF, Julier C, et al. Microcephaly and simplified gyral pattern of the brain associated with early onset insulin-dependent diabetes mellitus. *Neurogenetics* 2006;7:259–263
39. Poulton CJ, Schot R, Kia SK, et al. Microcephaly with simplified gyration, epilepsy, and infantile diabetes linked to inappropriate apoptosis of neural progenitors. *Am J Hum Genet* 2011;89:265–276
40. Shalev SA, Tenenbaum-Rakover Y, Horovitz Y, et al. Microcephaly, epilepsy, and neonatal diabetes due to compound heterozygous mutations in IER3IP1: insights into the natural history of a rare disorder. *Pediatr Diabetes* 2014;15:252–256
41. Fogli A, Boespflug-Tanguy O. The large spectrum of eIF2B-related diseases. *Biochem Soc Trans* 2006;34:22–29
42. Lin Y, Pang X, Huang G, et al. Impaired eukaryotic translation initiation factor 2B activity specifically in oligodendrocytes reproduces the pathology of vanishing white matter disease in mice. *J Neurosci* 2014;34:12182–12191
43. van der Knaap MS, van Berkel CG, Herms J, et al. eIF2B-related disorders: antenatal onset and involvement of multiple organs. *Am J Hum Genet* 2003;73:1199–1207
44. Shahmoradgoli M, Riazalhosseini Y, Haag D, et al. Protein phosphatase 1, regulatory subunit 15B is a survival factor for ER $\alpha$ -positive breast cancer. *Int J Cancer* 2013;132:2714–2719
45. Boyce M, Bryant KF, Jousse C, et al. A selective inhibitor of eIF2 $\alpha$  dephosphorylation protects cells from ER stress. *Science* 2005;307:935–939
46. Wiseman RL, Balch WE. A new pharmacology–drugging stressed folding pathways. *Trends Mol Med* 2005;11:347–350